Probing spin fractionalization with electron spin resonance based on scanning tunneling microscopy

Y. del Castillo [1,2] and J. Fernández-Rossier [1,*]

[1] *International Iberian Nanotechnology Laboratory (INL), Av. Mestre José Veiga, 4715-330 Braga, Portugal*

[2] *Centro de Física das Universidades do Minho e do Porto, Universidade do Minho, Campus de Gualtar, 4710-057 Braga, Portugal*

(Received 8 December 2023; revised 22 March 2024; accepted 11 July 2024; published 24 July 2024)

The emergence of effective $S = 1/2$ spins at the edges of $S = 1$ Haldane spin chains is one of the simplest examples of fractionalization. Whereas there is indirect evidence of this phenomenon, direct measurement of the magnetic moment of an individual edge spin remains to be done. Here we show how scanning tunnel microscopy electron-spin resonance (ESR-STM) can be used to map the stray field created by the fractional $S = 1/2$ edge spin and we propose efficient methods to invert the Biot-Savart equation, obtaining the edge magnetization map. This permits one to determine unambiguously the two outstanding emergent properties of fractional degrees of freedom, namely, their fractional magnetic moment and their localization length ξ.

DOI: 10.1103/PhysRevB.110.045145

I. INTRODUCTION

Fractionalization is one of the most dramatic examples of emergence in many-body systems [1–3]. It shows how new quantized degrees of freedom, such as quasiparticles with charge $e/3$, can govern the low-energy properties of a system of interacting electrons with charge e. In the case discussed here, a chain of interacting $S = 1$ spin behaves as if two $S = 1/2$ spin degrees of freedom were localized at the edges. These examples illustrate how it can not be ruled out that the quantum numbers of the so-called fundamental particles are actually emerging out of an interacting system made of degrees of freedom with different quantum numbers [4].

Haldane spin chains [5,6] provide one of the simplest examples of fractionalization and emergence. Out of a model of interacting $S = 1$ spins without intrinsic energy and length scales, a Haldane gap Δ_H, and two $S = 1/2$ degrees of freedom localized at the edges with localization length ξ emerge. Given that the building blocks of the model have $S = 1$, the $S = 1/2$ edge states are fractional. Their emergence can be rationalized in terms of the AKLT [7] valence bond solid state, which in turn has a number of outstanding properties, including being a resource state for measurement-based quantum computing [8].

The fractional charge of quasiparticles in the Fractional Quantum Hall effect was determined by an outstanding experiment [9,10] that leveraged on the relation between shot noise and charge [11]. In the case of spin fractionalization, a direct measurement of the spin of the fractional edge states and their localization length remains to be done. Until recently, experimental probes of Haldane spin chains relied on bulk probes, such as neutron scattering [12–16] and electron spin resonance [17–19], and provided indirect evidence of the presence of $S = 1/2$ degrees of freedom and a Haldane gap. Advances in on-surface synthesis combined with atomic-scale resolution inelastic electron tunnel spectroscopy (IETS) based on scanning tunnel microscopy (STM) have made it possible to probe individual Haldane spin chains made with covalently coupled $S = 1$ nanographene triangulenes [20]. IETS of triangulene spin chains showed the presence of a Haldane gap in the center of the chains as well as in-gap edge excitations for short chains and zero bias Kondo peaks for longer chains [20], consistent with the existence of emergent $S = 1/2$ edge spins [21]. However, a direct measurement of the edge magnetic moment $M = g\mu_B S_{\text{edge}}$ associated to the fractional $S_{\text{edge}} = 1/2$ degrees of freedom is missing. Here we design an experiment that exploits STM-based electron spin resonance (ESR-STM) [22] to unambiguously demonstrate spin fractionalization. We assume that a Haldane spin chain, not necessarily made with triangulenes, is deposited on a surface, sufficiently decoupled from the substrate so that the Kondo effect is suppressed, the magnetic moment of the edge states is preserved, and can be probed with ESR-STM magnetometry [23]. The feasibility of this weak-coupling scenario has been demonstrated in several ESR-STM experiments where $S = 1/2$ species, such as Ti [23–26], Cu [27], and alkali atoms [28], are deposited on a bilayer of MgO on top of an Ag surface.

Our proposal (see Fig. 1) relies on the demonstrated capability of ESR-STM to act as an absolute magnetometer [23,29]. To do so, an ESR-STM active spin acts as a sensor that can be placed at several distances of a second spin or group of spins denoted as target. At finite temperature, the target spins can occupy different quantum states, each of which generates its own stray field [23,30]. As a result, the ESR-STM spectrum of the sensor spin features several peaks, whose frequency and intensity relate to the stray-field and occupation probability of the quantum state of the target. As we show below, this can be used to obtain a direct measurement of the magnetic moment, and thereby the spin, of the edge states in Haldane spin chains.

*On permanent leave from Departamento de Física Aplicada, Universidad de Alicante, 03690 San Vicente del Raspeig, Spain; Contact author: joaquin.fernandez-rossier@inl.int

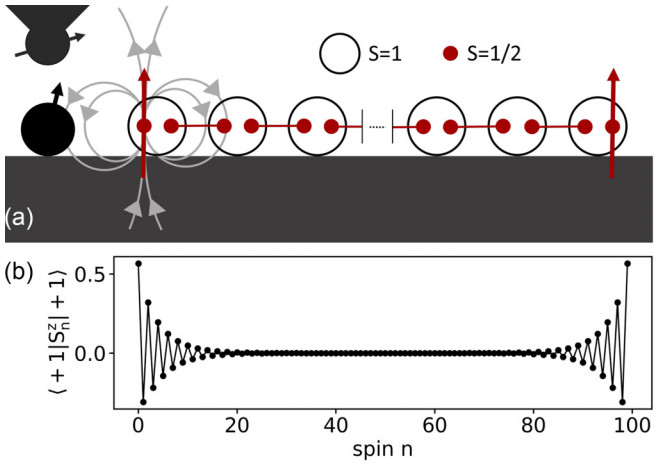

FIG. 1. (a) Scheme of the proposed experiment to measure fractionalization by means of ESR-STM. A Haldane chain is built on a kondo-free surface. The system is described as if there were two $S = 1/2$ objects at the edge. An ESR active atom (sensor atom) is placed near the chain to infer the magnetic moments of such chain from its stray field. (b) Spin density of the $S^z = +1$ triplet state for $\beta = 0.09$.

II. METHODS

A. Modeling Haldane spin chain

We assume that a Haldane spin chain with N spins $S = 1$ is placed on a surface. Recent experimental work reports the deposition of graphene ribbons on the MgO(100)/Ag(100) surface [31], suitable for STM-ESR. Given that Haldane spin chains have been made with nanographenes [20], this is a promising step. We also assume that the Haldane chain can be described with the Hamiltonian

$$\mathcal{H} = \sum_{n=1,N-1} J[\vec{S}_n \cdot \vec{S}_{n+1} + \beta(\vec{S}_n \cdot \vec{S}_{n+1})^2] + \sum_{n=1,N} g\mu_B \vec{S}_n \cdot \vec{B}. \quad (1)$$

We take values of β in the range $0 < \beta < \frac{1}{3}$. The low energy manifold is conformed by a singlet with $S = 0$ and a $S = 1$ triplet. The singlet-triplet splitting is given by the sum of the effective interedge coupling and the Zeeman energy:

$$E(S, S^z) = S\Delta_{ST}(N) + g\mu_B S^z B^z, \quad (2)$$

where μ_B is the Bohr magneton, $g = 2$ and $S = 0, 1$, and $S^z = \pm 1, 0$. We choose the quantization axis of the spin to be parallel to the external magnetic field.

The singlet-triplet splitting shows an exponential decay given by $\Delta_{ST} \propto e^{-N/\xi}$, where N is the system size and ξ represents the localization length. This quantity remains significantly smaller than the Haldane gap, the energy splitting between the low-energy manifold and the bulk states. The exponential dependence of Δ_{ST} closely resembles what would be expected if two $S = 1/2$ spins were localized at the edges of the chain, with a localization length on the order of ξ. This characteristic is illustrated in Fig. 1(b), where we calculate the expectation value of the S_n^z operators for the low-energy states with $S = 1$ and $S^z = +1$. Clearly, these states form a magnetic texture localized at each edge, with a combined magnetic moment of $S^z = \sum_{n=1,N/2}\langle \pm 1|S_n^z|\pm 1\rangle = \pm 1/2$.

B. STM-ESR magnetometry

We now consider that an STM-ESR-active spin picks up the straight field generated by a nearby Haldane spin chain. In ESR-STM experiments, the DC current across the STM-surface junction is measured as a function of the frequency of the driving voltage. The ESR-STM spectrum for this lateral-sensing setup can be described by the following equation [23,30]:

$$I_{DC}(f) = \sum_{\ell} p_\ell \mathcal{L}(f - f(\ell)), \quad (3)$$

where the sum runs over the eigenstates of the Hamiltonian [Eq. (1)] of the spin chain, $\mathcal{H}|\ell\rangle = E_\ell|\ell\rangle$, $p_\ell = \frac{1}{Z}e^{-E_\ell/(k_B T)}$ are the thermal occupations of each eigenstate and $\mathcal{L}(f - f_\ell)$ is a Lorentzian type resonance curve centered around the frequency f_ℓ. We assume that the external magnetic field is perpendicular to the sample so that the stray field created by the chain at the sensor location is also perpendicular to the substrate.

Since both the external field and the exchange interactions are much larger, it is safe to neglect the backaction effect of the stray field of the sensor on the Hamiltonian of the spin chain [35]. As a result, the resonant frequency of the sensor shifts linearly with the stray field:

$$f(\ell) = \frac{\mu_B g_s}{h}(B + b(\ell)), \quad (4)$$

where $h = 2\pi\hbar$, and g_s is the gyromagnetic factor of the sensor, and B and b_ℓ denote the external field and the stray field generated by the target spins in the state ℓ, respectively, both along the off-plane direction.

In turn, the stray field is given by

$$b^z(\ell) = -\frac{\mu_0}{4\pi}\sum_{n=1}^{N}\frac{m_n^z(\ell)}{(d^n)^3}, \quad (5)$$

where d^n is the distance between the sensor and the spin n. The magnetic moment vector $m_n^z(l)$ is generated by the spin n in each state ℓ, and its components are given by

$$m_n^z(\ell) = -g\mu_B\langle\ell|S_n^z|\ell\rangle. \quad (6)$$

Equations (3)–(6) relate the expectation value of the magnetic moments in a given Haldane-chain state $|\ell\rangle$ to the ESR-STM spectrum of a nearby sensor.

III. FRACTIONALIZATOIN VERIFICATION

We now discuss how to determine the magnetic moment of these states and verify fractionalization. Importantly, we assume that the temperature is much smaller than the Haldane gap [36], so that only the four states of the ground state manifold of the chain contribute to the sum in Eq. (3). Only two of these states, with $S = 1$ and $S^z = \pm 1$, have a nonvanishing expectation value of the spins. The corresponding magnetic profile of the $S^z = +1$ states calculated using DMRG [37–40], is shown in Fig. 1(b), for $\beta = 0.09$, relevant for triangulene spin chains [20,41]. It corresponds to two

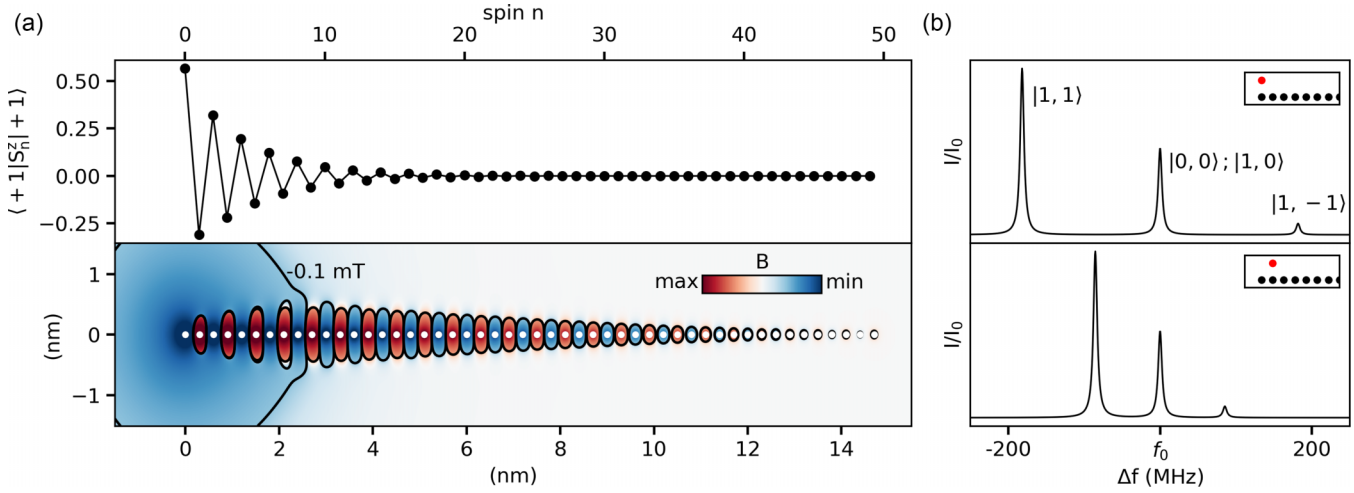

FIG. 2. (a) The top panel shows the $\langle S_z^n \rangle$ in the $S^z = 1$ state of the low-energy manifold for the first half of a Haldane chain of 100 spins with $S = 1$. The lower panel illustrates the z component of the stray field generated by the magnetic moments from the spins in the top panel (represented as white dots) on the xy plane. In this example, the chain is located spanning from $(x = 0, y = 0, z = 0)$ to $(x = +Na, y = 0, z = 0)$. Here, a represents the physical spacing between the $S = 1$ spins, treated as point particles. We choose $g = 2$ and a spacing of 0.3nm from each other. The contour lines highlight regions where the stray field has a magnitude of ± 0.1mT. (b) ESR spectra produced by the low-energy manifold states of the spin array described in panel (a), measured by sensors at different locations (red dots in the inset scheme). The sensors are located at a distance of 0.5 nm from the array. In this example, $J = 18$ meV, $T = 1$ K, $B_z = 1$, T, and $\beta = 0.09$.

physically separated objects with $S^z = 1/2$ localized at the edges. The $S^z = -1$ has analogous properties. In contrast, the expectation value of the spin operators is identically zero when calculated with the $S^z = 0$ states. Consequently, the four low-energy states of the Haldane spin chain correspond to three distinct magnetic states, with a vanishing stray field for the $S = 0$ and $S = 1, S^z = 0$ states, and a finite stray field of opposite sign for the $S^z = \pm 1$ states (see Fig. 2(a). As a result, the ESR-STM spectrum of the spin-sensor has three distinct peaks corresponding to three different stray fields (See Fig. 2(b). Expectedly, the stray fields of the $S^z = \pm 1$ have the same magnitude and opposite sign. From the splitting of these peaks, it is possible to pull out the value of the stray field at the location of the sensor:

$$b^z(\pm 1) = \frac{h}{g_s \mu_B}(f_0 - f_{\pm 1}) \tag{7}$$

here, $f_{\pm 1}$ represents the resonant frequencies measured at the sensor when the Haldane spin chain occupies the states with $S^z = \pm 1$ within the ground state manifold.

A. Inversion of the Biot-Savart equation

In order to determine the magnetic moments of the $N/2$ spins of one half of the chain, that define a vector $\mathcal{M} \equiv (m_1(\pm), ..., m_{N/2}(\pm))$, we need to measure the stray field in a set of different locations N_M, that yields a vector in the readout-location space, $\mathcal{B} \equiv (b_1(\pm), ..., b_{N_M}(\pm))$. We have considered two methods to pull out the vector $\mathcal{M}$ out of $\mathcal{B}$. The first method is the full inversion of the Biot-Savart's equation (FIBS), that can be written down as $\mathcal{B} = -(\mu_0/4\pi)\mathbf{D}\mathcal{M}$, where the elements of the matrix $\mathbf{D}$ are $|d_{n_m}^n|^{-3}$. In this case, it is apparent that the number of necessary readouts equals half of the chain length, $N_M = N/2$. The second method involves the use of machine learning models and requires a dramatically smaller number of measurements to determine the magnetization map (Figs. 3(c) and 3(d).

B. Inversion of the Biot-Savart equation and estimation of sensitivity

The finite magnetic sensitivity of the readouts, denoted by $\delta\mathcal{B}$, imposes an uncertainty in the determination of the edge magnetic moment. The sensor spectral resolution is ultimately limited by the shot noise [35]:

$$\delta B_{\min} = \frac{4}{3}\frac{h\delta f}{g_s \mu_B}\sqrt{\frac{e}{I_0 \Delta t}}, \tag{8}$$

where δf is the linewidth, I_0 is the maximal current in the resonance peak, and Δt is measurement time, which may be limited by factors such as thermal drift of the tip. The associated minimal shift in the sensor frequency given by $\Delta f \min = g\mu_B \delta B_{\min}/h$ in the range of 1 MHz have been reported in STM-ESR magnetometry [23].

In the case of the FIBS, the uncertainty of the edge magnetic moments is given by

$$\delta\langle S^z \rangle = \left(\frac{4\pi}{\mu_0 \mu_B g}\sum_{n,n_m}\left|(\mathbf{D}^{-1})_{n_m}^n\right|\right)\delta B_{\min}. \tag{9}$$

In Fig. 3(a), we show that assuming the reported resolution, $\Delta f \min = 1$ MHz [23], the uncertainty in the determination of the edge spin, $\delta\langle S^z \rangle$, is an order of magnitude lower than $\langle S^z \rangle$. In principle, longer readout times would make it possible to decrease δf, and thereby, $\delta\langle S^z \rangle$.

C. Inversion of the Biot-Savart using machine learning

We now discuss a second method to invert the Biot-Savart equation that makes use of machine learning-based numerical

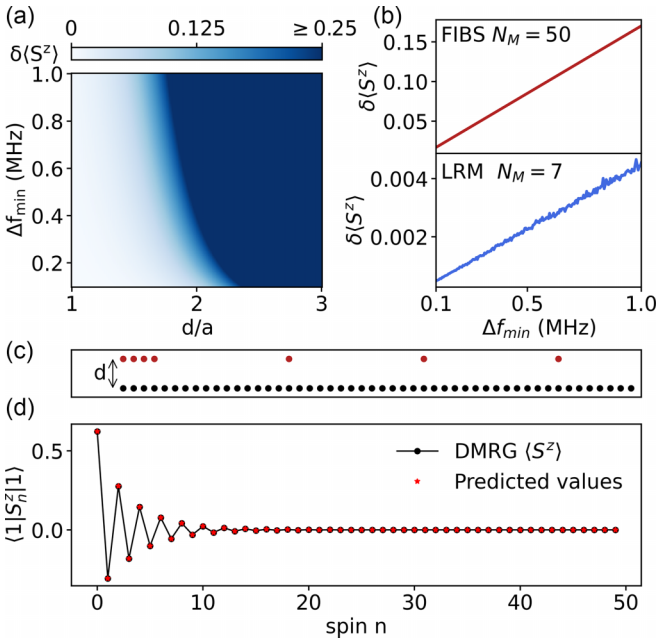

FIG. 3. (a) $\delta\langle S^z\rangle$ as a function of both the perpendicular distance of the N_m sensors to the chain (d) and the spectral resolution $\Delta f_{\min}$ for a $S = 1/2$ sensor, with $N_m = N/2$ different locations from $(x = 0, y = d)$ to $(x = +N_m a, y = d)$. (b) Error comparison between linear inversion of the Biot-Savart's equation (FIBS) in the top panel and linear regression model (LRM) using $N_m = 7$ sensor positions ($d = 0.5$ nm) in the bottom panel. (c) Location of the sensor positions of the NN configuration (red dots) near the spin chain (black dots). (d) LRM prediction of the expectation values of the spins using a magnetic profile with noise compared to the original values.

methods to invert Biot-Savart's equation. This method comes with two advantages. First, it reduces the number of ESR-STM measurements. Second, it yields a smaller uncertainty in the determination of the fractional spin. Our approach involves two different machine learning methods. The first one is a neural network model that classifies magnetic profiles derived from ESR readouts, confirming the presence of the characteristic Haldane spin chain edge magnetization [see Fig. 1(b)].

The second is a linear regression model (LRM) with machine learning trained coefficients to convert Haldane-type magnetic profiles, with a specific number of measurements, into spin expectation values. The training set incorporates several thousand spin distributions obtained varying β between 0 and 1/3, each with its characteristic magnetic profile. In addition, we added random noise with amplitude bounded by the magnetic sensitivity range (see the Supplemental Material [35]). The synergistic use of these two machine learning methods together allows it to be trained in a few minutes on a conventional laptop. This is crucial since a distinct model needs to be trained for each experimental layout, considering factors such as spin arrangement, sensor positions, sensor type, and spectral resolution.

In Fig. 3(b), we used $N_M = 7$ strategically positioned measurements [35], as shown in Fig. 3(c). Our calculations reveal that, with a number of ESR readouts much smaller than $N/2$, it is possible to obtain the magnetization maps and, therefore, the total magnetic moment of half of the chain with uncertainty as low as $\delta\langle M_z\rangle/\Delta f_{\min} \approx 10^{-2}\mu_B/MHz$ (see the Supplemental Material [35]), as shown in Fig. 3(b). Consequently, this methodology proves sufficient for determining the presence of an $S = 1/2$ object and its localization length, using state-of-the-art ESR-STM instrumentation.

D. Determination of localization length

We now discuss how to infer another important property of the edge spins, namely, their localization length ξ. This is based on two facts. First, the inversion of the Biot-Savart equation yields the value of the magnetic moment at many sites close to the edge. Second, our numeric work shows that we can parametrize the spins with the following equation:

$$\langle S_n^z\rangle_{\pm} = \pm(-1)^n \mathcal{A} e^{-\frac{n}{\xi}}, \tag{10}$$

where $\mathcal{A}$ represents the maximum value of $\langle S_n^z\rangle$ at the edge spin, ensuring that $\sum_{n=1}^{N/2}\langle S_n^z\rangle = \frac{1}{2}$ [42]. Our numerical calculation (see the Supplemental Material [35]) shows that the second moment of the magnetization field $\langle n\rangle = \frac{\sum_n |\langle S_n^z\rangle|\cdot n}{\sum_n |\langle S_n^z\rangle|}$ is proportional to ξ in an almost one-to-one relation ($\langle n\rangle \approx 1.02\,\xi$), which permits one to determine this quantity with an uncertainty associated to $\delta\langle S_n^z\rangle$. For the reported spectral resolution of 1 MHz and d=0.5 nm, the relative errors would be $\frac{\delta\xi}{\xi} \approx 10^{-1}$ for FIBS and $\frac{\delta\xi}{\xi} \approx 10^{-3}$ for LRM. [35].

IV. CONCLUSION

In conclusion, we propose a method to measure the two outstanding properties of the $S = 1/2$ fractional degrees of freedom that emerge at the edges of Haldane $S = 1$ chains: their fractional magnetic moment $M = g\mu_B S$ and their localization length or spatial extension, ξ. Our theoretical analysis shows that our method can be implemented with state-of-the-art ESR-STM magnetometry. Our proposal permits one to go beyond previous work, where the presence of fractional degrees of freedom is inferred indirectly, but the actual fractionalization of the magnetic moment is not measured directly. This approach could be used to probe fractional edge spins expected to occur in two-dimensional AKLT models and could also inspire similar experiments using related atomic scale magnetometers, such as NV centers [43–48] and ESR-AFM [49]. We also note that recent work [50], reporting the implementation of STM-ESR with the resonating spin located at the tip, rather than on the surface as considered here, would simplify the determination of fractionalization significantly, removing the need to carry out on-surface atomic manipulation of the sensor.

ACKNOWLEDGMENTS

We acknowledge Arzhang Ardavan for fruitful discussions and Jose Lado for technical assistance on the implementation of DMRG. J.F.-R. acknowledges financial support from FCT (Grant No. PTDC/FIS-MAC/2045/2021), Generalitat Valenciana funding Prometeo2021/017 and MFA/2022/045, and funding from MICIIN-Spain (Grants No. PID2019-109539GB-C41 and No. PID2022-141712NB-

C22). Y.D.C. acknowledges funding from FCT, QPI, (Grant No. SFRH/BD/151311/2021) and thanks the hospitality of the Departamento de Física Aplicada at the Universidad de Alicante.

[1] W.-P. Su, J. R. Schrieffer, and A. J. Heeger, Phys. Rev. B **22**, 2099 (1980).
[2] D. C. Tsui, H. L. Stormer, and A. C. Gossard, Phys. Rev. Lett. **48**, 1559 (1982).
[3] R. B. Laughlin, Phys. Rev. Lett. **50**, 1395 (1983).
[4] R. B. Laughlin and D. Pines, Proc. Natl. Acad. Sci. USA **97**, 28 (2000).
[5] F. Haldane, Phys. Lett. A **93**, 464 (1983).
[6] F. D. M. Haldane, Phys. Rev. Lett. **50**, 1153 (1983).
[7] I. Affleck, T. Kennedy, E. H. Lieb, and H. Tasaki, Phys. Rev. Lett. **59**, 799 (1987).
[8] T.-C. Wei, I. Affleck, and R. Raussendorf, Phys. Rev. Lett. **106**, 070501 (2011).
[9] L. Saminadayar, D. C. Glattli, Y. Jin, and B. Etienne, Phys. Rev. Lett. **79**, 2526 (1997).
[10] R de-Picciotto, M. Reznikov, M. Heiblum, V. Umansky, G. Bunin, and D. Mahalu, Phys. B: Condens. Matter **249**, 395 (1998).
[11] C. L. Kane and M. P. A. Fisher, Phys. Rev. Lett. **72**, 724 (1994).
[12] W. J. L. Buyers, R. M. Morra, R. L. Armstrong, M. J. Hogan, P. Gerlach, and K. Hirakawa, Phys. Rev. Lett. **56**, 371 (1986).
[13] Z. Tun, W. J. L. Buyers, R. L. Armstrong, K. Hirakawa, and B. Briat, Phys. Rev. B **42**, 4677 (1990).
[14] T. Yokoo, T. Sakaguchi, K. Kakurai, and J. Akimitsu, J. Phys. Soc. Jpn. **64**, 3651 (1995).
[15] I. A. Zaliznyak, S.-H. Lee, and S. V. Petrov, Phys. Rev. Lett. **87**, 017202 (2001).
[16] M. Kenzelmann, G. Xu, I. Zaliznyak, C. Broholm, J. F. DiTusa, G. Aeppli, T. Ito, K. Oka, and H. Takagi, Phys. Rev. Lett. **90**, 087202 (2003).
[17] L. C. Brunel, T. Brill, I. Zaliznyak, J. P. Boucher, and J. P. Renard, Phys. Rev. Lett. **69**, 1699 (1992).
[18] C. D. Batista, K. Hallberg, and A. A. Aligia, Phys. Rev. B **60**, R12553(R) (1999).
[19] A. I. Smirnov, V. N. Glazkov, T. Kashiwagi, S. Kimura, M. Hagiwara, K. Kindo, A. Y. Shapiro, and L. N. Demianets, Phys. Rev. B **77**, 100401(R) (2008).
[20] S. Mishra, G. Catarina, F. Wu, R. Ortiz, D. Jacob, K. Eimre, J. Ma, C. A. Pignedoli, X. Feng, P. Ruffieux, J. Fernandez-Rossier, and R. Fasel, Nature (London) **598**, 287 (2021).
[21] F. Delgado, C. D. Batista, and J. Fernández-Rossier, Phys. Rev. Lett. **111**, 167201 (2013).
[22] S. Baumann, W. Paul, T. Choi, C. P. Lutz, A. Ardavan, and A. J. Heinrich, Science **350**, 417 (2015).
[23] T. Choi, W. Paul, S. Rolf-Pissarczyk, A. J. Macdonald, F. D. Natterer, K. Yang, P. Willke, C. P. Lutz, and A. J. Heinrich, Nat. Nanotechnol. **12**, 420 (2017).
[24] T. S. Seifert, S. Kovarik, D. M. Juraschek, N. A. Spaldin, P. Gambardella, and S. Stepanow, Sci. Adv. **6**, eabc5511 (2020).
[25] M. Steinbrecher, W. M. J. van Weerdenburg, E. F. Walraven, N. P. E. van Mullekom, J. W. Gerritsen, F. D. Natterer, D. I. Badrtdinov, A. N. Rudenko, V. V. Mazurenko, M. I. Katsnelson, A. van der Avoird, G. C. Groenenboom, and A. A. Khajetoorians, Phys. Rev. B **103**, 155405 (2021).
[26] P. Kot, M. Ismail, R. Drost, J. Siebrecht, H. Huang, and C. R. Ast, Nat. Commun. **14**, 6612 (2023).
[27] K. Yang, P. Willke, Y. Bae, A. Ferrón, J. L. Lado, A. Ardavan, J. Fernández-Rossier, A. J. Heinrich, and C. P. Lutz, Nat. Nanotechnol. **13**, 1120 (2018).
[28] S. Kovarik, R. Robles, R. Schlitz, T. S. Seifert, N. Lorente, P. Gambardella, and S. Stepanow, Nano Lett. **22**, 4176 (2022).
[29] F. D. Natterer, K. Yang, W. Paul, P. Willke, T. Choi, T. Greber, A. J. Heinrich, and C. P. Lutz, Nature (London) **543**, 226 (2017).
[30] Y. del Castillo and J. Fernández-Rossier, Phys. Rev. B **108**, 115413 (2023).
[31] S. Kovarik, R. Schlitz, A. Vishwakarma, D. Ruckert, P. Gambardella, and S. Stepanow, Science **384**, 1368 (2024).
[32] J. M. Taylor, P. Cappellaro, L. Childress, L. Jiang, D. Budker, P. Hemmer, A. Yacoby, R. Walsworth, and M. Lukin, Nat. Phys. **4**, 810 (2008).
[33] A. Dréau, M. Lesik, L. Rondin, P. Spinicelli, O. Arcizet, J.-F. Roch, and V. Jacques, Phys. Rev. B **84**, 195204 (2011).
[34] J. F. Barry, J. M. Schloss, E. Bauch, M. J. Turner, C. A. Hart, L. M. Pham, and R. L. Walsworth, Rev. Mod. Phys. **92**, 015004 (2020).
[35] See Supplemental Material http://link.aps.org/supplemental/10.1103/PhysRevB.110.045145 for a numerical estimate of the back action of the sensor; derivation of Eq. (8); details of the two machine learning models approach, the guidelines for sensor positions, and its errors; numerical calculation of the relation between localization length and the second moment; and its uncertainties, which includes Refs. [32–34].
[36] We note that, for the case of nanographene Haldane spin chains, the range of temperatures where ESR-STM has been implemented with, $T < 4K$, is much smaller as Δ_H was found to be in the range of 10 meV.
[37] S. R. White, Phys. Rev. Lett. **69**, 2863 (1992).
[38] S. R. White and D. A. Huse, Phys. Rev. B **48**, 3844 (1993).
[39] G. Catarina and B. Murta, Eur. Phys. J. B **96**, 111 (2023).
[40] J. Lado, DMRGpy library (2023).
[41] J. C. G. Henriques and J. Fernández-Rossier, Phys. Rev. B **108**, 155423 (2023).
[42] We note that the spatial dependence of either Kondo peak amplitude is proportional to $|\langle S_n^z\rangle_\pm|^2$, and could be used in principle to obtain the localization length. However, the proposed method is much more accurate, as being linear in the magnetization.
[43] G. Balasubramanian, I. Y. Chan, R. Kolesov, M. Al-Hmoud, J. Tisler, C. Shin, C. Kim, A. Wojcik, P. R. Hemmer, A. Krueger, T. Hanke, A. Leitenstorfer, R. Bratschitsch, F. Jelezko, and J. Wrachtrup, Nature (London) **455**, 648 (2008).

[44] M. S. Grinolds, S. Hong, P. Maletinsky, L. Luan, M. D. Lukin, R. L. Walsworth, and A. Yacoby, Nat. Phys. **9**, 215 (2013).
[45] L. Rondin, J.-P. Tetienne, T. Hingant, J.-F. Roch, P. Maletinsky, and V. Jacques, Rep. Prog. Phys. **77**, 056503 (2014).
[46] S. Chatterjee, J. F. Rodriguez-Nieva, and E. Demler, Phys. Rev. B **99**, 104425 (2019).
[47] Z. Liu, J. Li, R.-Z. Huang, J. Li, Z. Yan, and D.-X. Yao, Phys. Rev. B **105**, 014418 (2022).
[48] A. Finco and V. Jacques, APL Mater. **11**, 100901 (2023).
[49] L. Sellies, R. Spachtholz, S. Bleher, J. Eckrich, P. Scheuerer, and J. Repp, Nature (London) **624**, 64 (2023).
[50] T. Esat, D. Borodin, J. Oh, A. J. Heinrich, F. S. Tautz, Y. Bae, and R. Temirov (unpublished).